ISSN No. 0737-5352-11

Annual Report on Studies of Space/Time Variability of Marine Boundary Layer Characteristics

Contract No. N00014-86-C-0459

Thomas H. Vonder Haar, Principal Investigator

December 1987

CIRA Cooperative Institute for Research in the Atmosphere

Colorado State University

[CIRA paper no. 11]

Annual Report for 1987
from the
Cooperative Institute for Research in the Atmosphere
Colorado State University

to

Marine Meteorology Section
Ocean Sciences Division
of the
Office of Naval Research

on

Studies of Space/Time Variability
of
Marine Atmospheric Boundary Layer Characteristics

Contract #N00014-86-C-0459

Thomas H. Vonder Haar, Principal Investigator

March, 1988

TABLE OF CONTENTS

		Page
1.0	Introduction	1
2.0	Coastal Stratus Experiment	2
	2.1 Meteorological and Microphysical Observations	2
	2.2 Radiative Measurements of MABL Clouds	11
	2.3 Radiative Transfer Modeling	14
3.0	Cloud Cover Statistics	18
4.0	Dynamical Modeling of Radiation Effects	26
5.0	Summary of Preliminary Results	30
	Acknowledgements	32
	References	33
	Appendix A Summary of Data from the Coastal Stratus Experiment	35
	Appendix B Cumulative List of Reports, Publications and Presentations	45
	Appendix C Graduate Student Support	46

1.0 Introduction

The objectives of this research program include (1) development of remote sensing techniques for characterizing the marine atmospheric boundary layer (MABL); and (2) study of the space–time variability in MABL cloud structure under the influence of meteorological conditions and radiative forcing. Work toward these objectives during the first sixteen months of the contract covers three phases, defined as (1) analysis of *in situ* radiative, thermodynamic and microphysical data obtained during a Coastal Stratus Experiment (CSE) near San Diego; (2) determination of cloud cover statistics from full-resolution and reduced-resolution satellite archival data; and (3) limited use of a new very high resolution MABL model to explore aspects of stratus cloud variability. Preliminary results concern the influences that cloud structure and aerosol from marine, continental and anthropogenic sources exert on radiative transfer in the MABL. Results on sampling requirements for existing satellites, and the potential of new observations in near-infrared wavelengths, have also been obtained.

Contributions to this report have been made by graduate students Melanie Wetzel and Chi-Fan Shih, and CIRA Postdoctoral Fellow Hung-chi Kuo.

2.0 Coastal Stratus Experiment

Characterization of the Marine Atmospheric Boundary Layer (MABL) over broad regions using satellite data requires detailed *in situ* measurements to validate the physical interpretation of the satellite data. A new technique with potential for estimating cloud droplet size from satellite observations would utilize cloud radiance measurements in the near-infrared water vapor window wavelengths, in particular, 1.6 μm. Remote estimates of cloud droplet effective radius could have several applications, for example in the parameterization of cloud radiative properties such as single scattering albedo and asymmetry parameter (Slingo and Schrecker, 1982). Thus, a field measurement program was carried out during the last two weeks of June, 1986 near San Diego, California. With the cooperation of the Naval Ocean Systems Center (NOSC), an instrumented aircraft (Jensen, 1978) was flown in areas of coastal stratus at different times during the daylight hours to measure broadband and spectral solar radiation above and within the MABL (Wetzel and Vonder Haar, 1986a). Observational equipment on board the twin-engine Piper Navajo aircraft is listed in Table 1. Data obtained during the field experiment were then used in radiative transfer modeling of cloud spectral reflectance, and the relationship of cloud reflectance to droplet sizes and cloud structure was evaluated.

2.1 Meteorological and Microphysical Observations

Experimental flight periods are given in Table 2, during which some or all of the instruments were operated. Satellite digital data from the GOES-6 VISSR and NOAA-9 AVHRR image sensors were recorded over the study region. Analysis of the GOES satellite imagery utilized the CIRA Interactive Research Imaging System (IRIS) to map and display the area of interest.

The satellite imagery provides an encompassing look at the study region during the transition from morning cloud cover to breakup near the coast. The size and spacing of cloud elements increases throughout the image area during the day. Figure 1 through Figure 3 present this variability. A

Table 1: Instrumentation Used on Navajo Aircraft in June 1986.

	Instrument	Measured Parameters
1.	Rosemount Temperature Probe	Air Temperature
2.	EG & G Model 137 - C3 Cooled-Mirror Hygrometer	Dew Point
3.	Rosemount Model 542K Pressure Altimeter	Pressure Altitude
4.	LORAN-C	Latitude/Longitude
5.	PMS Axially Scattering Spectrometer Probe - Model 100	Particle size distributions (0.23 - 14.7 μm radius)
6.	PMS Optical Array Probe - Model 200	Particle size distributions (14.2 - 150 μm radius)
7.	Eppley Precision Spectral Pyranometers	Near-infrared and total shortwave fluxes, upward and downward
8.	CI Spectral Radiometer	Upward radiance in 6 milliradian field-of-view, for narrow band shortwave filters centered at 0.65, 0.85, and 1.6 micrometers

Table 2: Aircraft measurement periods during June 1986.

Date	*Julian day*	*Time period (UTC)*
24 June	175	2012–2201
25 June	176	2202–2340
26 June	177	1523–1744
27 June	178	0132–0250
28 June	179	1406–1445
28 June	179	1555–1612
29 June	180	1420–1755
30 June	181	1418–1757

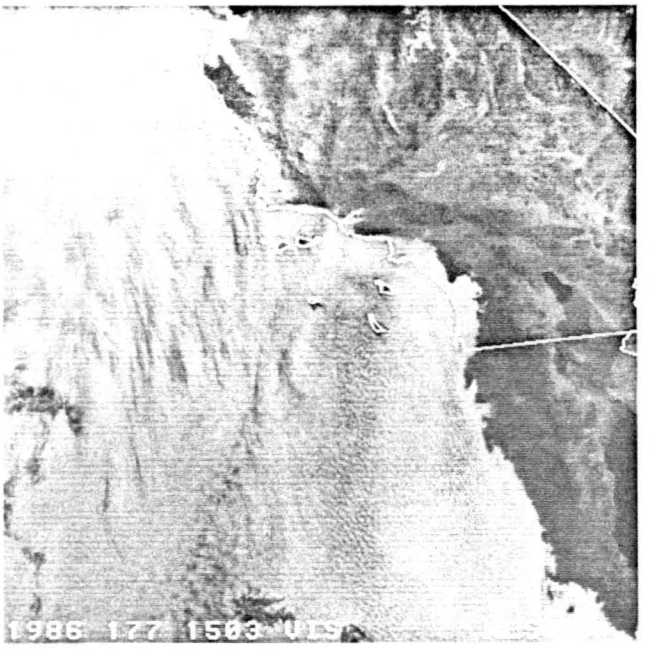

Figure 1: Satellite image from early morning of day 177.

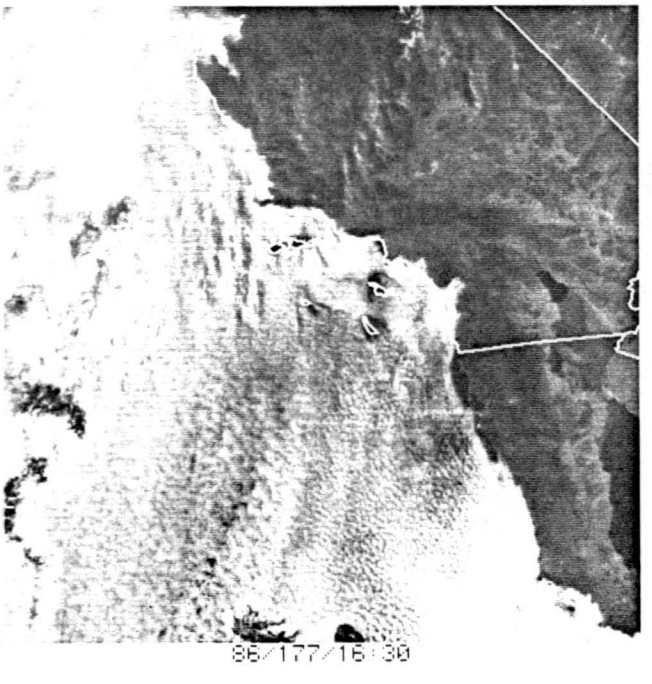

Figure 2: Satellite image from morning of day 177.

zoomed view of the GOES image depicts the cloud structure and sampling areas during the morning (0930 PDT) in Figure 4.

A one-kilometer spatial cloud scale is below the resolution of the GOES infrared image sensor (4 km by 8 km). The AVHRR infrared resolution is much more suitable for stratus cloud studies. This data showed effective temperatures for the stratus tops and the ocean surface to be within 3°C. Infrared imagery during the night hours indicate the filling in of cloud cover to the coast, and slight decrease in cloud top temperature associated with overcast conditions.

Analyses of the boundary layer cloud and thermodynamic structure are included in Appendix A of this report. Synoptic rawinsonde data were also recorded, as well as hourly surface meterological observations. The coastal land–sea breeze is marked by weak off-shore flow during the early morning and a shift to stronger, on-shore flow as the day progresses. The 12-hourly sounding profiles depict the persistent and strong subsidence inversion, which is more precisely defined with the aircraft measurements of temperature and dew point during sampling flights (see Appendix A). The dew point depression above the inversion increases from approximately 20°C to 30°C during the night, while air temperature at these heights remains fairly constant. Absolute humidity develops a minimum value within the inversion, which is notably lower than during the afternoon (1 g/ks vs. 4 g/kg or more). These observations indicate that mixing with cloudy air is suppressed and moisture is not being supplied to moisten the inversion layer during the night hours.

During the research flights, cloud layer conditions ranged from continuous overcast stratus to broken stratocumulus fields with fractional coverage $\approx$ 60%, and cloud depths were observed as $<$150 m. Most of the clouds appeared to have low liquid water content, and cloud base was ill-defined. No precipitation was encountered below cloud. Only mild turbulence was experienced, in the form of a very occasional updraft or downdraft. Varying degrees of aerosol contamination were observed below the boundary layer inversion. The horizontal delineation of this layer was visible by coloring of the air below, and was consistantly and significantly more distinct when looking toward land than toward the open ocean. The color, and smell detectable from inside the aircraft when

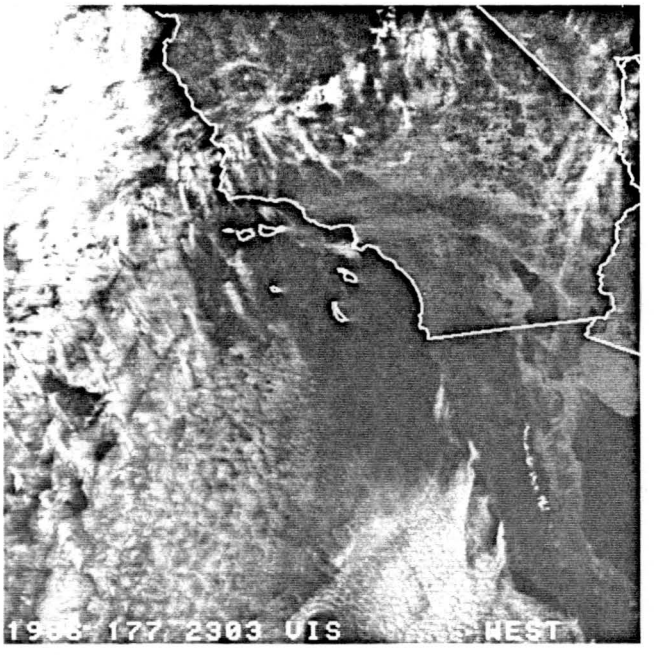

Figure 3: Satellite image from afternoon of day 177.

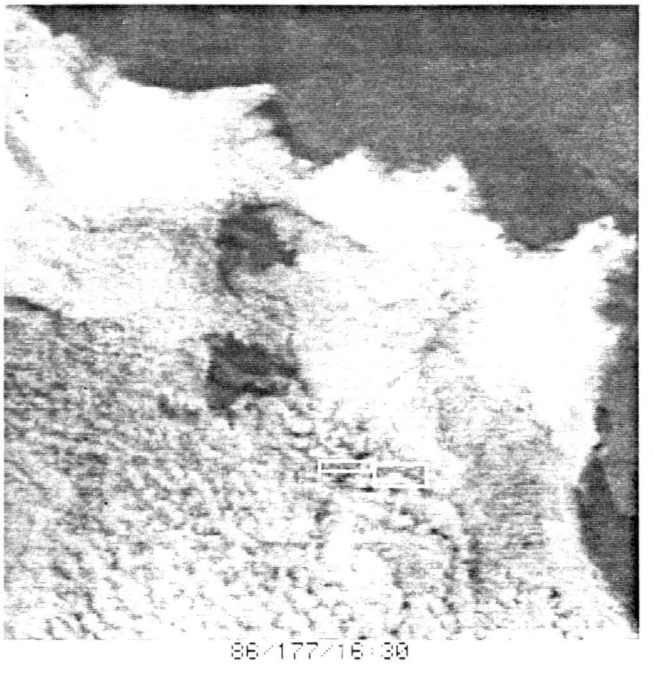

Figure 4: Expanded view of image at 1630 UTC on day 177.

near the urbanized area, indicated pollutant aerosol would have been mixing with marine haze in the near-shore region.

In general, the stratus layers sampled during the field program were characterized by small mean and effective droplet radii. Large particle concentrations were due to inclusion of the aerosol population, with the smallest particles assumed to be counted by the ASSP have the radius 0.23 μm. The cloud top sampling altitudes which passed in and out of cloud top contain the most frequent occurrence of small r_e, large N, and small W grouped with obvious cloud air (larger r_e, moderate N, and large W).

Aerosol within the cloud layer is also contributed by sea spray through the lower cloud boundary. A sampling pass obtained very near the ocean surface during day 178 suggests the ocean as source of available CCN, with large concentrations of aerosol-size particles. The decrease of particle concentrations from up to 700 cm^{-3} at 100 feet MSL to no more than 350 cm^{-1} at 400 feet MSL implies that less than half of the generated CCN may reach cloud base altitudes. According to work by Bottalino *et al.* (1982), aerosol concentrations *near the ocean surface* at this locale typically exceed 10^3 cm^{-3} for radii $< 0.5\mu$m when the prevailing flow is marine, and on the order of 10^2 cm^{-3} for a continental airmass.

Individual samples of the droplet size distribution (DSD) included many instances where significant numbers of large droplets were found. Measurements from tethered balloon in stratocumulus reported by Caughey and Kitchen (1984) found that large drops were preferentially located in discrete plumes of downward convection presumed to originate from radiatively cooled air at cloud top. The presence of individual DSD samples with both smaller and larger effective radii than the majority strongly suggests turbulent exchange in the top 100–200 feet of the cloud layer. Similar variation near cloud base occurred in a more restricted vertical extent. It is important to realize, however, that the relatively low sampling frequency provided an entire size spectrum only every eight seconds. During this sampling time, the aircraft travels 430 meters. The analysis of these data was accomplished by averaging within the cloud along constant-altitude flight paths, while individ-

ual eight-second samples that were considered to be within cloud elements were selected from the cloud-top passes.

Evidence of size modes was recorded in the droplet distributions, most notably at cloud top. The DSD modes at large sizes (10 and 15 μm) were generally accompanied by relatively fewer aerosol-sized particles. The presence of aerosol size modes ($N > 10^3$ cm$^{-3}\mu$m^{-1}) was marked by lower numbers of the large droplets. Considerably more uniformity in the size distributions was encountered while fully in cloud. Fluctuations in r_e along the constant-altitude flight tracks were generally less than 2.0 μm, except for those flight levels immediately at cloud upper and lower boundaries, during which the PMS probes were in and out of cloudy parcels during the sampling time. Significant reduction in the numbers of droplets larger than 5 μm radius was only found in updrafts.

Averaging of droplet size distributions along constant-altitude flight segments reveal a decrease in the mean value of the effective radius at lower altitudes below cloud top. The mean values and dispersion (D; ratio of standard deviation to mean) for effective radius, liquid water content, and number concentration are listed in the tables of Appendix A. Droplet sizes and liquid water content near cloud top remained essentially similar for each of the flights in cloud. Diurnal transitions were manifest primarily in the percentage cloud cover, due to cloud evaporation and break-up during the day. Most of the flights showed that liquid water content and effective radius increased toward cloud top, reaching maxima of $W \approx 0.1$ g m^{-3} and $r_e \approx 6$ μm.

The presence of an entrainment interface layer (EIL) above marine stratocumulus is discussed by Nicholls and Turton (1986). This has depth of a few tens of meters, within which a significant proportion of the mixing between cloud air and inversion air takes place. The haze overlying the cloud layer during some of the sampling periods suggested the same type of interface. Mixing of air parcels near the cloud top could be indicated by the larger variation of r_e and W shown at the cloud top altitudes in Figure 5 and Figure 6, which were derived from droplet size distributions without the aerosol component.

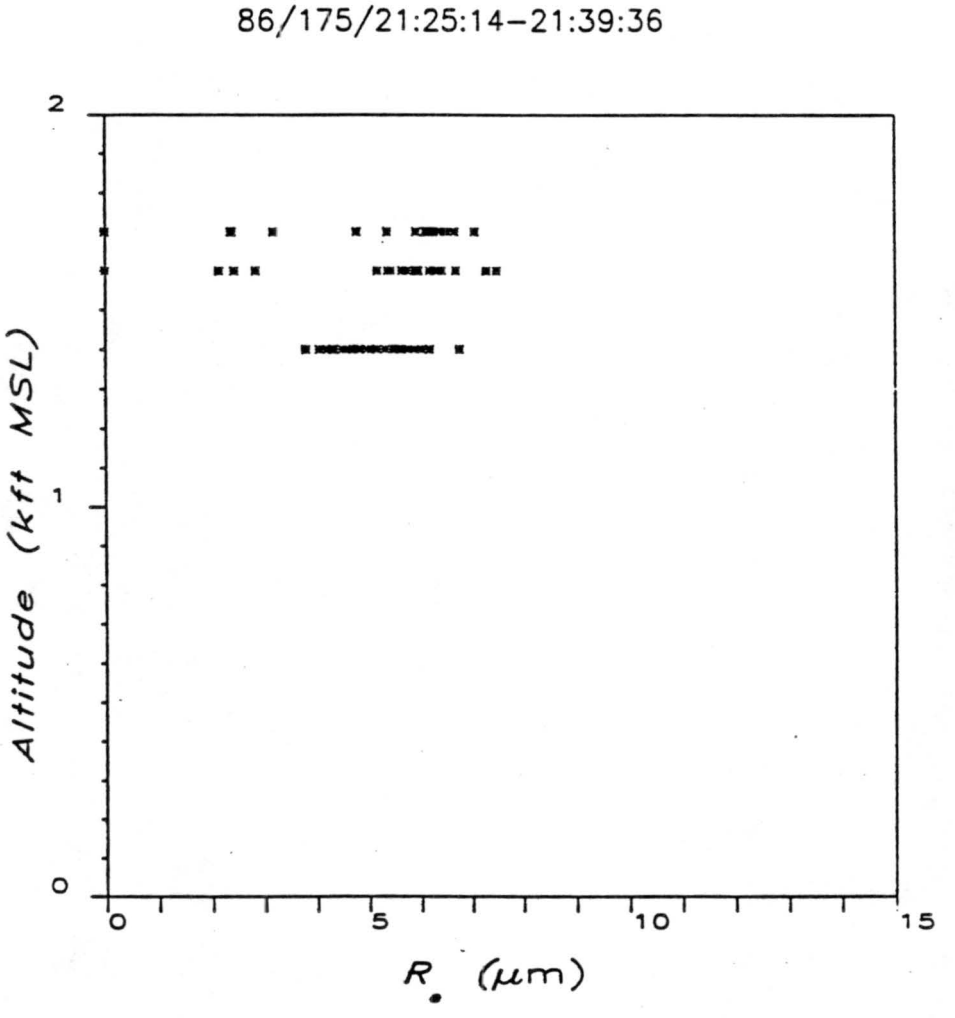

Figure 5: Effective radius sampled during flight 175A, without the aerosol size ranges.

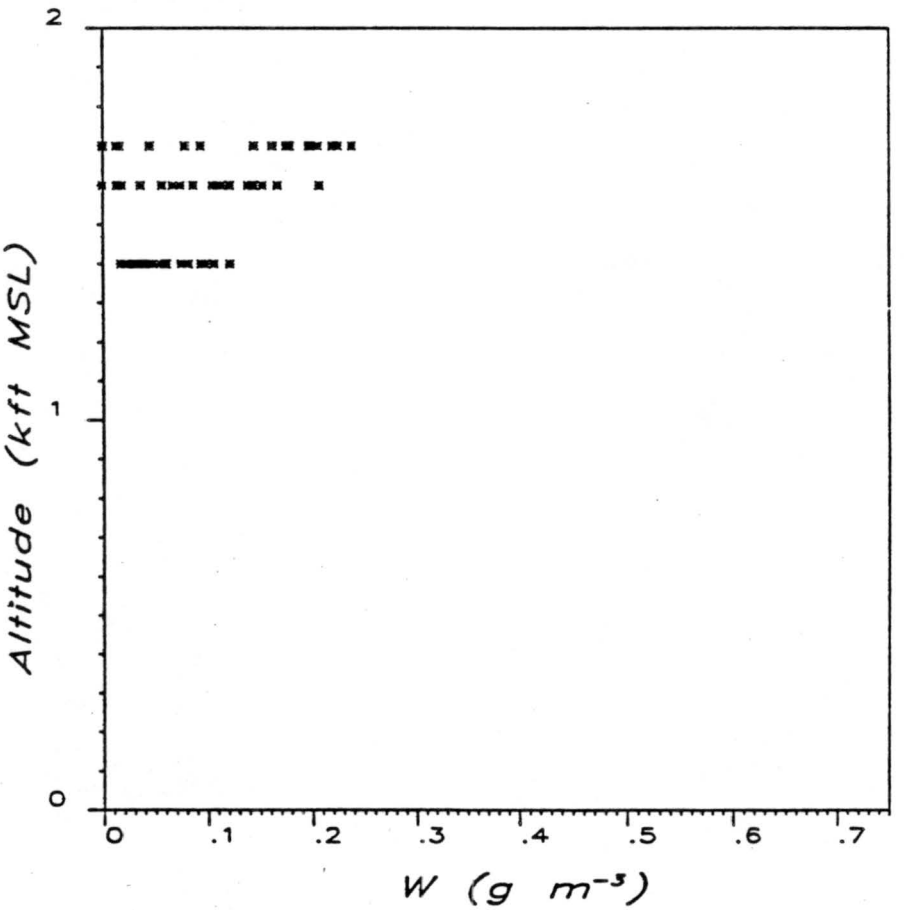

Figure 6: Liquid water content sampled during flight 175A, without the aerosol size ranges.

The broad droplet spectrum suggested for shallow convection confined within only a portion of the boundary layer by Nicholls and Leighton (1986) appears in the sampling which occurred in the early morning. During these two flight sequences the liquid water content and droplet sizes displayed maxima in the lower part of the cloud, with the largest values exceeding $W = 0.5$ g m^{-3} and $r_e = 11\mu$m. However, these were overlain by the cloud top region with a diminished droplet size distribution. These clouds were more fog-like at 0830 local time than those sampled later. The influence of radiational cooling during the previous night may have suppressed mixing with the overlying inversion air. That the largest droplets were found in the lower cloud during the flight may be explained by settling of the largest sizes since the strong radiational cooling mechanism had been "turned off" two hours earlier at sunrise. A time of approximately two hours for gravitational settling through the upper cloud layer was calculated from the terminal velocity of the larger droplets.

2.2 Radiative Measurements of MABL Clouds

Following the results of a plane-parallel radiation model, which indicate a relationship between effective cloud droplet sizes and spectral reflectance in the near-infrared water vapor "window" bands, the droplet size distributions sampled in the coastal stratus have been compared with the spectral radiance patterns. A plane-parallel radiative transfer model based on the adding-and-doubling method (AD) (Grant and Hunt, 1968) has been used to simulate vertical cloud structure and the extinction effects of aerosol (Wetzel and Vonder Haar, 1986b). The field observations near the San Diego coast included periods of heavy aerosol loading.

The spectral reflectance is defined as a directional reflectance factor for hemispherical incidence over a narrow wavelength interval. It is calculated from

$$\rho_\lambda = \frac{\pi L_\lambda^+}{E_\lambda^-} \tag{1}$$

where λ denotes the narrow spectral bandwidth (or monochromatic wavelength) for which the calculation is valid. L_λ^+ is the upward spectral radiance at a specified quadrature angle which represents

the viewing zenith angle of a sensor aloft. The term in the denominator is the downward spectral irradiance.

The sensitivity of estimates for downwelling spectral irradiance in the visible and NIR windows to variations in aerosol and water vapor were examined using the LOWTRAN-6 atmospheric transmission model, which incorporates specific extinction parameters for aerosol (marine haze, tropospheric aerosol, and stratospheric aerosol) and atmospheric gases (Kneizys *et al.*, 1983). Assuming the sun-target-sensor geometry is known and the climatological atmospheric profile is chosen, the probable error of LOWTRAN flux estimates is primarily controlled by the boundary layer profile.

Field measurements of downwelling solar flux agreed closely with the LOWTRAN estimates to altitudes above the inversion, but sharp decreases in solar flux (up to 20%) were recorded as the aircraft moved from above to below the inversion, due to smog and haze occurring near the coast. These variations were reproducible in the LOWTRAN estimates only by using the "marine aerosol" model options of LOWTRAN. While these options are intended just for such applications, it is also necessary to have a vertical sounding which locates the height of the boundary layer. The signal values recorded in the Spectral Radiometer channels also suggested that the percentages of irradiance associated with the two longer-wavelength window channels (0.85 and 1.6 μm) remained constant, while the 0.65-μm band suffered extinction in the inversion layer air above cloud top. Remote sensing methods may have greater problems with the visible band, if spectral irradiance is determined wholly from estimates.

In contrast to the behavior in and near the visible, cloud reflectance within the longer wavelength NIR windows shows significant effects of cloud droplet absorption as the droplet size distributions are altered. The asymptotic values of $\rho_{1.6}$, as well as their relative magnitudes at limited optical depths, decrease as the effective radius of the DSD increases. The same behavior is noted at 2.15 μm. The separation of reflectances according to effective radius improves as the optical depth increases, then levels off for extreme optical thicknesses. The variation of reflectance with optical depth changes as the sensor view angle is moved from near-vertical to larger angles, but the difference between

reflectances for two given droplet size distributions remains nearly constant. At a known sun-cloud-sensor geometry, the reflectance relationship is consistent.

The clouds for which spectral radiance measurements were obtained exhibited quite small optical depths. The comparison of measured cloud radiance to radiative transfer calcuations is therefore limited to a regime of low reflectance. Unfortunately, the measured values of cloud reflectance were still significantly smaller than would be expected from clouds of the observed depths and droplet size characteristics (for example, a measured value of 3% versus a model calculation of 20%). For this reason, the absolute calibration for the SR is suspect. However, the ratio of reflectances in pairs of the filter channels could still be determined.

The value of the ratio

$$R_{0.85}^{1.6} = \frac{\rho_{1.6}}{\rho_{0.85}} \tag{2}$$

is expected to be greater than unity for cloud layers of limited depth and limited absorption (such as the stratus water clouds). Due to the increased absorption for droplet size distributions with large r_e values, the ratio $R_{0.85}^{1.6}$ should be comparitively smaller for that type of cloud layer than for those characterized by a small effective radius. This conclusion applies to layers with *equivalent* scaled optical depths, rather than the same physical depth.

The values of these ratios obtained from the field data are consistently less than unity. Similar results can be obtained by evaluating the same ratio from three stratocumulus case studies discussed by Stephens and Platt (1987) (SP). In these case studies, the measured ratio was less than unity, even though a detailed adding model produced results which predict the ratio to be equal to 1.08 and 1.21 for the two cases of small optical thickness (δ = 6 and 5, respectively). The third case ($\delta = 10$) when modelled, showed a predicted ratio equal to 0.85, while the measured ratio was again considerably less (0.65). Twomey and Cocks (1982) also report discrepancies between modeled and measured spectral reflectances over stratocumulus, although the sense of disagreement is opposite to those data described above. Possible reasons for the low values of measured reflectance at 1.6 μm compared to 0.85 μm were exlored using the radiative transfer models.

An associated set of data from this sampling is the ratio of 0.65-μm to 0.85-μm reflectances. At altitudes above the cloud *and* inversion, this ratio was often smaller than unity, while above cloud but within the inversion, the ratio was larger than one. This implied that significant extinction at 0.65 μm was occurring within the inversion, which further supports the contention that window measurements at this wavelength may be ambiguous due to unknown gaseous and/or particulate extinction. Similar differences in $R_{0.85}^{1.6}$ above versus below the haze layer were not noted.

2.3 Radiative Transfer Modeling

Results of "adding" (using the AD plane-parallel model) two stratus cloud layers with different DSD's show that an estimated value of droplet size is more representative of the cloud as a whole, rather than the cloud top layer. If the typical marine stratus layer demonstrates an increase in droplet size toward cloud top, then the cloud should be darker in the near-infrared than would be assumed from internal cloud size distributions. However, simulations which matched the sampled cloud layers did not produce strong darkening.

We compared model reflectance for a group of DSD's with results of SP. Their calculated values of 1.6-μm reflectance were obtained from detailed multi-layer representations for three cloud decks, including gaseous absorption which may have minor effects in the chosen spectral bands. The effective radii of the upper cloud region for the SP cases were very close to that for Stratus 2. This suggests that the AD model represents these multilayer cases well. The values of reflectance *measured* at the top of these clouds was much less than their calculated results. The lower reflectance would imply a larger effective radius for the cloud, which neither the SP model nor the AD model have predicted. The influence of non-pure water composition for the DSD's has not been addressed in either of these results. Therefore, the refractive index variations potentially occuring in the aerosol and droplet populations is explored in the next section.

Refractive index variations designed to represent the aerosol populations were included in a set of the AD model runs. First, aerosol refractive indices were used to simulate an aerosol layer overlying a cloud droplet layer. For these cases, the aerosol size distribution was obtained by clear-air sampling

a short distance above cloud top (flight level 1.8 kft on day 177). Refractive indices were taken from Hänel (1976) to represent a strongly absorbing urban aerosol layer at low ambient relative humidity. The wavelength dependance of pure water cloud layers is not sufficient to produce the larger extinction at 1.6 μm, and is the addition of aerosol layers at cloud top was not effective enough in reducing cloud reflectance. For example, $\rho_{1.6}$ at 8° viewing angle decreases only slightly with the introduction of aerosol. A corresponding increase in optical depth offsets this, which otherwise may have been interpreted as a shift in the r_e characteristics of the layer.

A second source of data on aerosol refractive indices was Shettle and Fenn (1979). These refractive index data were used to simulate multicomponent droplet populations. A Stratus 2 distribution and the sampled DSD's provided the models, from which an aerosol component (radii less than two micrometers) and a droplet component (all larger sizes) were separated. Refractive indices for the various aerosol types in a 99% or lower relative humidity environment have been applied to the aerosol component, and indices for pure water have been assumed for the droplet size component. The primary difference is in the imaginary refractive index, which can be much larger for certain aerosol than for pure water.

An AD simulation of the single-layer cloud with the refractive index of oceanic aerosol at 99% RH for aerosol and droplet components has an asymptotic value (at large optical depth) of 0.51, compared to 0.57 for water cloud alone, with the sun at 50° zenith angle and the observer viewing from near nadir. At an optical depth of 8, $\rho_{1.6}$ for these clouds is 0.33 and 0.35. As in some of the results from the aerosol layering above cloud, the darkening is compensated by a decrease in scaled optical depth. Hence, the ratio of 0.85- and 1.6-μm reflectances remains essentially the same.

The incorporation of refractive indices of oceanic aerosol into the entire droplet population provides a means of explaining the reduction in reflectance at 1.6 μm. Under the assumption that cloud droplets growing within the marine boundary layer will continue to collect aerosol, the reduction in the aerosol indices during condensation could be limited. Therefore, a calculation was performed with the weighting of DSD refractive index equal to a homogeneous mixture of sea salt (15% con-

tribution) and pure water (85% contribution). AD model results using the Mie phase functions of droplet distributions with these larger refractive indices show that the ratio $R_{0.85}^{1.6}$ is markedly reduced. Taking the droplet size distribution in the upper cloud layer during sampling on day 177, we find that cloud reflectance at 1.6 μm would have been reduced by more than 11%. Because the real refractive index is constant (between 1.6 and 0.85 μm) for these cases, and the imaginary index is extremely small at 0.85 μm, the reflectance at 0.85 μm is only slightly reduced. Thus the reflectance ratio is diminished from 1.13 to 1.04. This reduced value is still larger than measured values. Various other assumptions concerning the droplet consituents and their refractive indices could be made, but due to lack of chemical measurements of these properties the actual compositions of droplets and aerosol could not be modeled. A test of the effect of including urban and rural aerosol showed large extinction at $\lambda = 0.85$ as well as at $\lambda = 1.60$, so that $R_{0.85}^{1.6}$ was not decreased. In order to explore other possible controls on spectral reflectance properties, the radiative modeling of broken cloud fields was pursued.

The three-dimensional radiative transfer model known as the Monte Carlo method for photon paths was implemented on the Cyber 205 computer in addition to the CIRA VAX systems, for the purpose of simulating broken stratus cloud fields. This was employed in determining if non-homogeneous cloud structure influences cloud reflectance in the window bands. The method utilized for this study is termed a "backward" scheme because it traces photons back from the collecting point (sensor) through a specified number of scattering interactions. The philosophy and implementation of this procedure is similar to that described by Collins *et al.* (1972). The computer code is based on that which was developed by Davis *et al.* (1985).

The Mie version of the adding model matched the Monte Carlo model well in point comparisons for the thin cloud layers. Several different cloud simulations have been made with the Monte Carlo model. Comparisons of upward-directed radiance at varied viewing angles have been made between plane-parallel (PP) and broken cloud fields. The results indicate that the reflectance of a cloud within a scattered field of other similar clouds (1 km in width and seperated by 1 km clear air) has

nearly the same reflectance as the PP layer. Secondly, this similarity occurs at 0.85 μm as well as at 1.6 μm and 2.1 μm. Even for a 0.5-km isolated cloud, loss of near-nadir radiance to the cloud edges is calculated as only 1%. The optical depth of this cloud is 4 in the vertical and 25 in the horizontal, which may account for the small loss of horizontally-directed energy. Similar results were obtained by Davies (1978) for cuboidal clouds of limited vertical and horizontal extent. Therefore, the horizontal inhomogeneity of these thin stratocumulus does not appear to be responsible for the unexpectedly low values of 1.6-μm reflectance.

Continued work on the effects of cloud structure and composition on spectral radiance patterns is being pursued. The overall effects of aerosol concentrations and composition was concluded to be small in altering the relationship of near-infrared reflectance to cloud droplet size. Horizontal variations due to thin patches or breaks in the cloud layer also have limited effect, based on model simulations. However, the measurements of lowered reflectance in the 1.6 μm band, discussed above, suggest an enhancement in extinction which should be taken into account and studied when satellite observations in this band are available soon from the AVHRR-K/L/M satellite series.

3.0 Cloud Cover Statistics

Diurnal variations in effective cloud top temperatures for boundary layer cloud are found (Shih and Vonder Haar, 1986) in the open ocean regions off both California and Peru (see Figures 7 and 8).

Observation of nighttime cooling of the cloud top is accompanied by increased cloud cover. During the day, cloud cells separate, and more cloud-free area is seen. This is manifest by broadening of pixel brightness histograms, with a larger population of dark (cloud-free) pixels at late afternoon image times. We are developing a multi-year stratus/stratocumulus cloud climatology utilizing data sets archived at CIRA. We recorded full-resolution GOES imagery during the DYCOMS Experiment (30 July – 21 August 1985), Coastal Stratus Experiment (24 June – 30 June 1986) and FIRE Experiment (23 June – 20 July 1987). ISCCP visible (at a reduced resolution of 8 km per pixel) and infrared image data are archived every three hours on a continuous basis. Summary and study of fractional cloudiness, characteristic cloud cell size, and cell spacing will be possible with the several sampling times per day. Sampling biases of GOES data must be acknowledged (Shih *et al.*, 1986) since cloud elements may not be spatially resolved, but the geostationary satellites provide information on transitions between cloud regimes not now available from the polar-orbiting satellites. Figures 9 and 10 contrast the visual differences between cloud patterns for VISSR full-resolution and ISCCP sampled data sets.

As we are developing our multiple-year stratus/stratocumulus cloud climatology based on the GOES VISSR data, we recongize the sampling and resolution biases of VISSR instrument. To help solve these difficulties, we have worked with Dr. Durkee at Naval Postgraduate School to obtain NOAA-9 AVHRR data during the Coastal Stratus Experiment. Using both VISSR and AVHRR data of the same observation time over the same geographical areas, we have started the comparisons of cloud analysis results from both data sets. Figures 11 to 16 are satellite images of VISSR and AVHRR channels for one of the Coastal Stratus Experiment. Twelve target regions were chosen for this case study as shown in Figures 11 to 16, and the cloud conditions within every target regions are different.

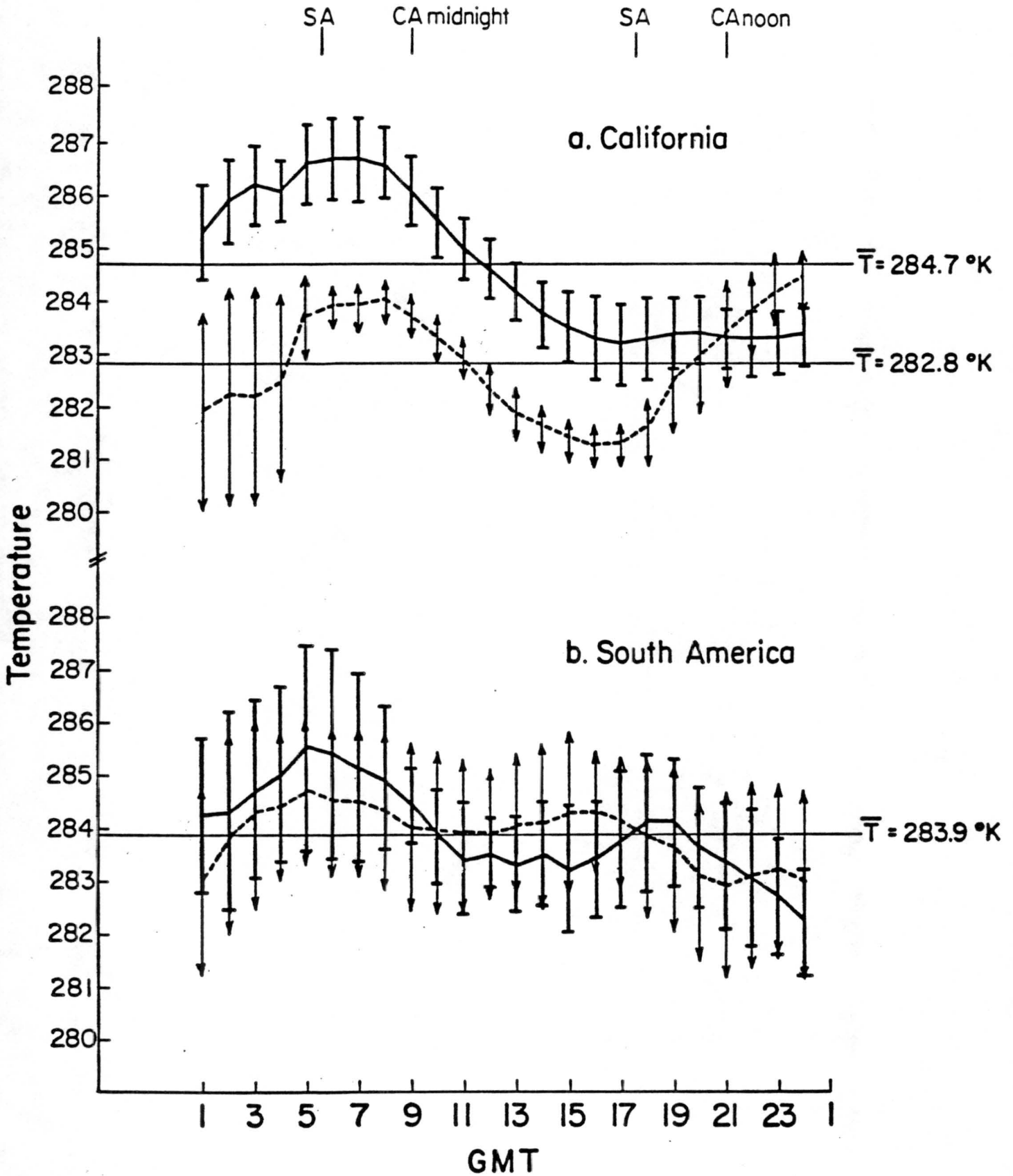

Figure 7: Mean standard deviation of effective temperature for 2.5° latitude/longitude regions of persistant stratocumulus near coastal California and Peru. The solid lines are sampled from areas further equatorward (southern California and northern Peru) than areas represented by the dashed lines (off of northern California coast and southern Peru).

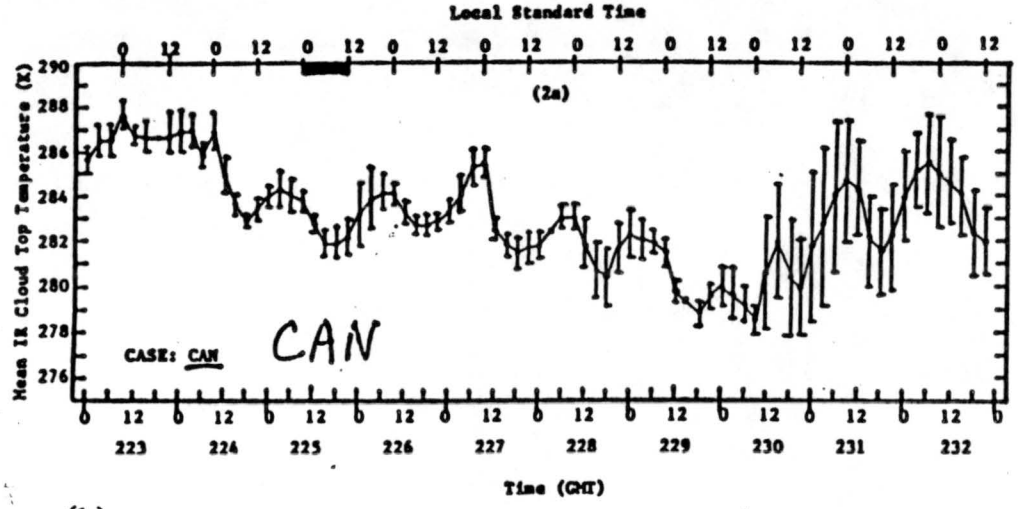

(b)

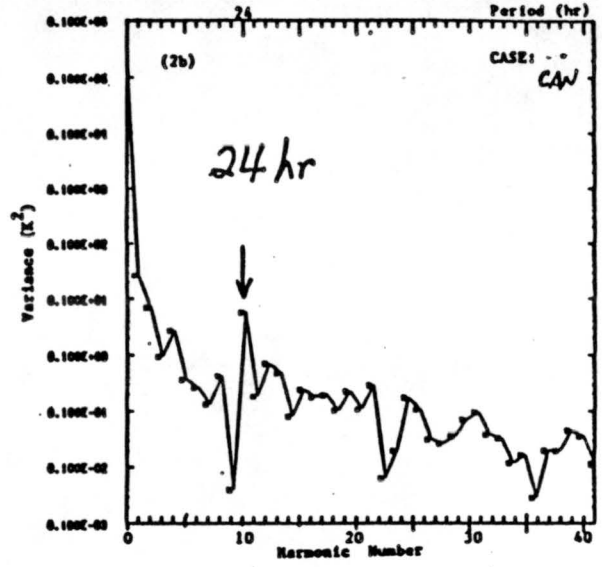

(c)

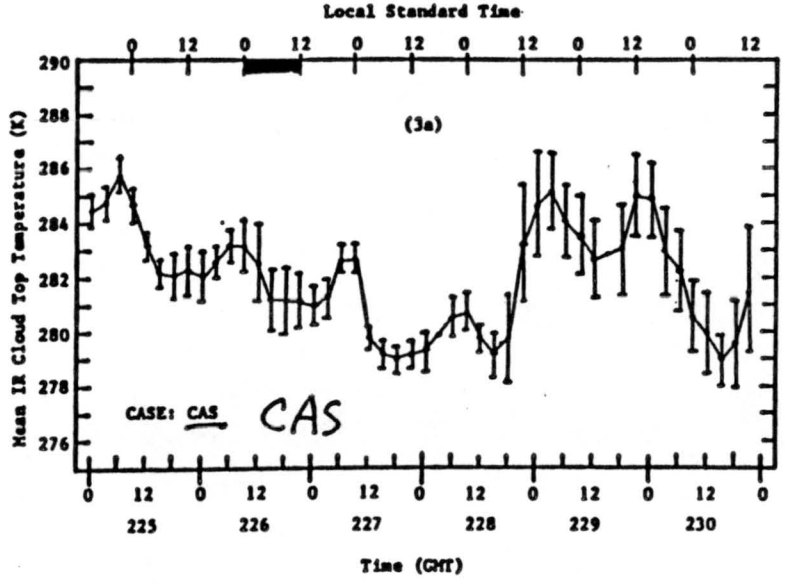

(a)

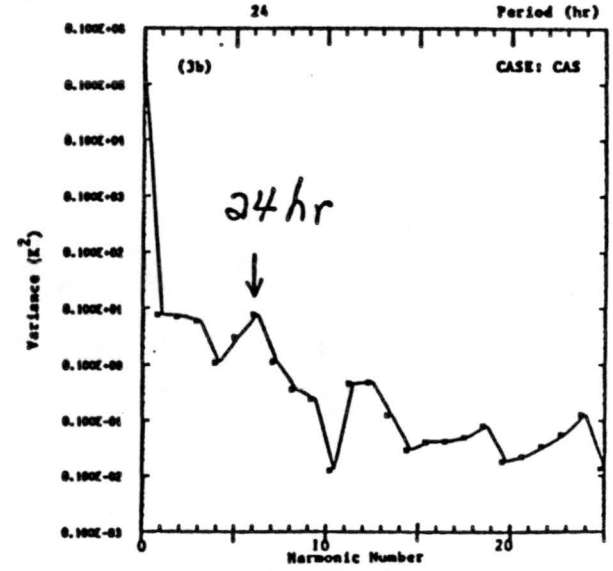

(d)

Figure 8: (a) and (b) Mean and standard deviation of effective temperature for stratocumulus off the coast of southern (CAS) and northern (CAN) California. (c) and (d) Harmonic analyses indicating a significant amount of explained time variance at a frequency of 24 hours.

Figure 9: Cloud patterns observed in GOES visible imagery at full resolution (2 km per pixel) and sampled for the ISCCP continuing data archive (8 km).

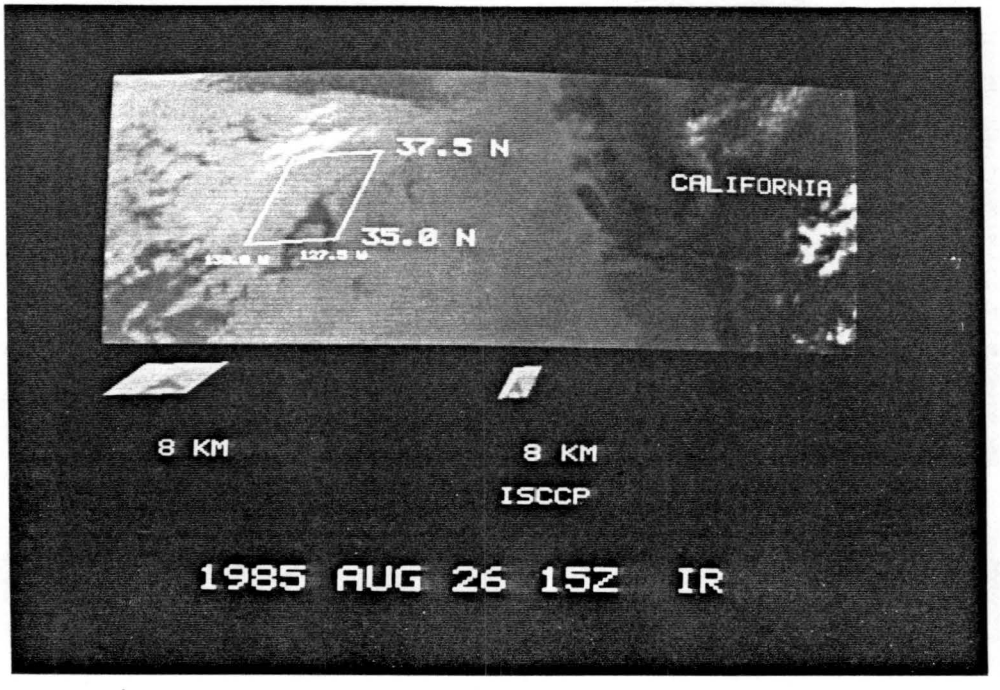

Figure 10: As in Figure 9, for infrared imagery with raw data resolution (4 km x 8 km) and ISCCP sampled resolution (12 km x 8 km).

Figure 11: Visible channel of GOES VISSR data for 26 June 1986 2300Z. Twelve target regions (A–L) are shown.

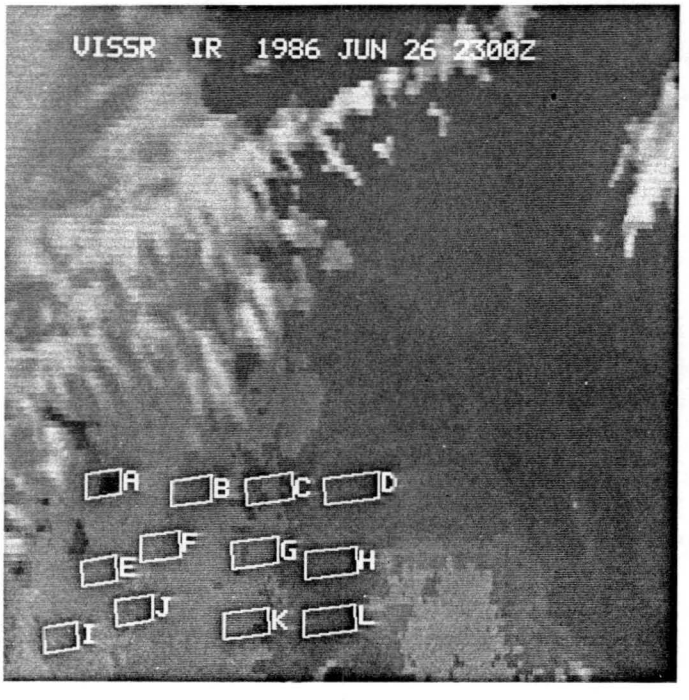

Figure 12: Same as Figure 11 but for infrared channel.

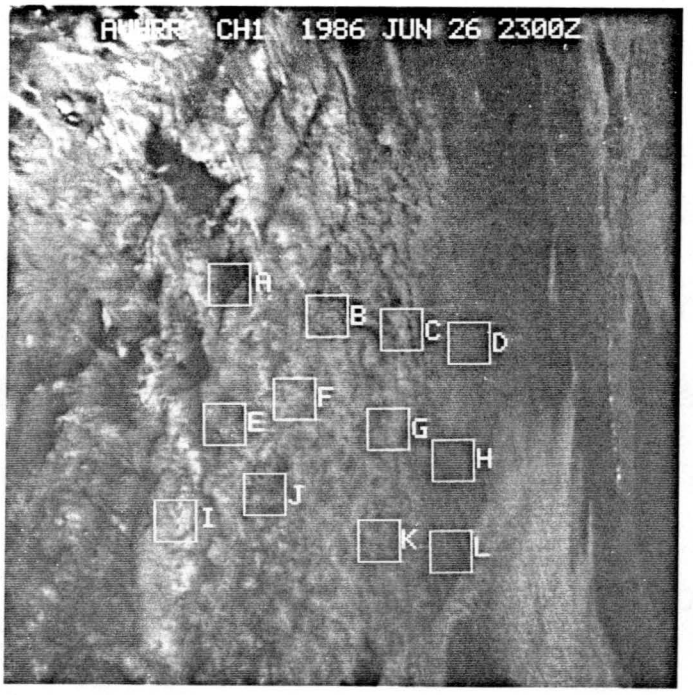

Figure 13: Channel 1 of AVHRR data for the same time as in Figure 11.

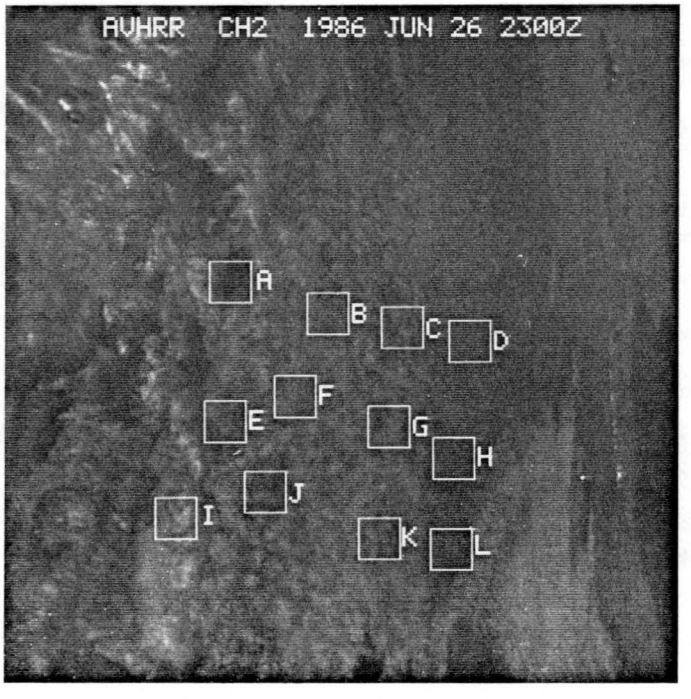

Figure 14: Same as Figure 13 but for Channel 2.

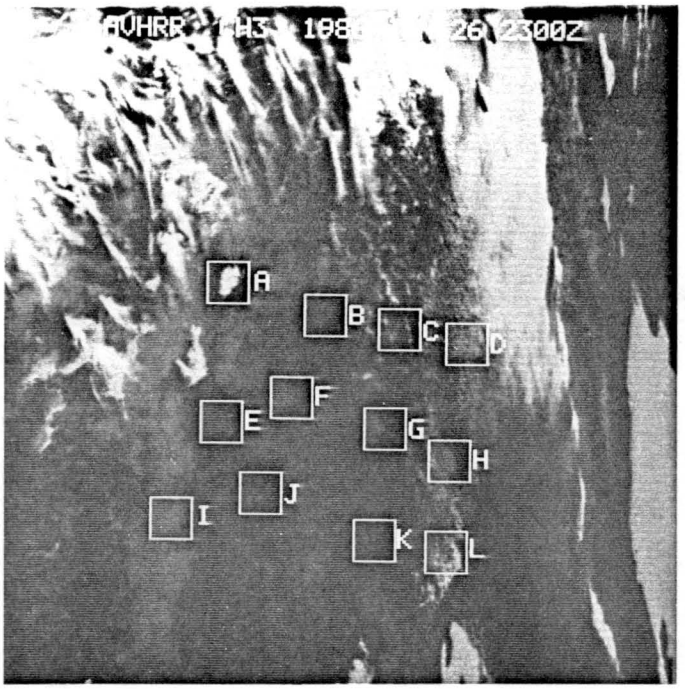

Figure 15: Same as Figure 13 but for Channel 3.

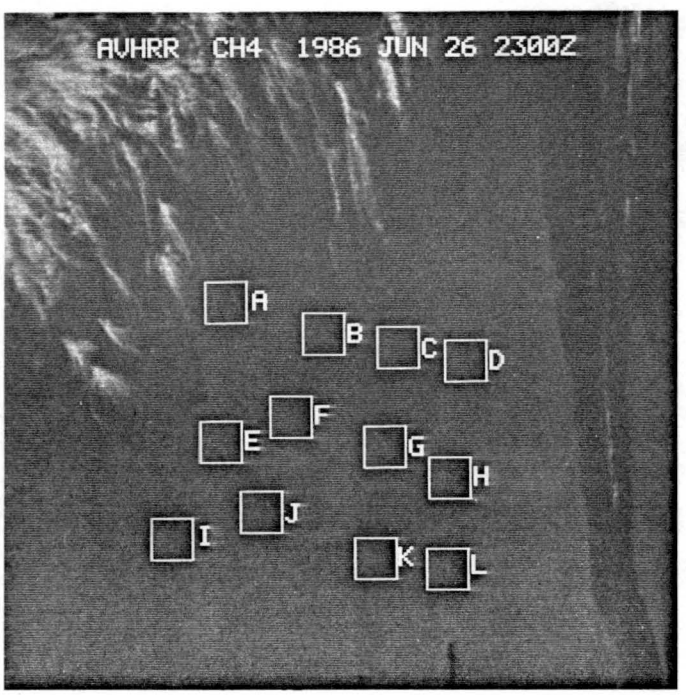

Figure 16: Same as Figure 13 but for Channel 4.

Region A is clear in the center, while regions B, C, E, F, G, J, and K are mostly cloudy with different textures. Regions D, H and L are located near the boundary of stratus/stratocumulus areas. Region I is mostly cloudy with vigorous turrets. Our analyses of this case study will include cloud top temperature, shortwave reflectance, and cloud fractions at different spatial resolutions derived from both VISSR and AVHRR data sets. The results will be presented (Shih *et al.*, 1988) at the American Meteorological Society's Third Conference on Satellite Meteorology and Oceanography Anaheim, California during 31 January – 5 February 1988. The overall conclusion from this study is that full resolution visible data from the satellites is needed for determining basic cloud cover statistics near the edges of extended stratocumulus fields and in areas of enhanced convection. Within the extended cloud region, small area (8 or 16 km) averaging can be performed prior to statistical summaries in order to reduce data processing requirements for the stratus cloud climatology. We will next develop an objective method for identifying whether a given image area is to be sampled at full or reduced resolution.

4.0 Dynamical Modeling of Radiation Effects

A two-dimensional Boussinesq moist model has been developed to investigate the interaction between dynamics and infrared radiation in the cloud-topped marine boundary layer (Kuo, 1987). A spectral tau numerical method and high resolution (10 meters per grid space) provide the accuracy and detail necessary to simulate cloud top processes. Model domain is 2500 m in the horizontal and 800 m in the vertical. The spatial discretization is Fourier-Galerkin in the horizontal and Chebyshev-tau in the vertical. Time integration follows a fourth-order Runge-Kutta scheme with four second time steps. The initial conditions consist of a well mixed boundary layer 450 m in depth with a 100 m deep inversion. The cloud layer extends from 200 m to 450 m, with adiabatically determined liquid water content (increasing nearly linearly with height). Model conditions matched the field observations of the Coastal Status Experiment quite closely.

The initial vertical profiles were time integrated under different radiative forcings (see Figure 17). The first four placed the infrared cooling within the cloud layer, with two of these directly dependant on local liquid water content. The two forcings not dependant on local conditions were assigned horizontally uniform cooling rates. A fifth experiment assigned a layer of cooling directly above the cloud. This experiment may be interpreted as a simulation of an above-cloud haze layer with a strong negative infrared net flux due to water and aerosol constituents.

The results indicate that the dynamical evolution of the cloud-topped marine boundary layer do not depend on the horizontal or vertical distribution of cooling when confined to the turbulent boundary layer. Radiational cooling of an air parcel does not occur on a shorter time scale than the internal circulation. Figures 18 and 19 show the velocity fields and liquid water distributions resulting from a water content-based cooling experiment and the above-cloud cooling experiment, respectively. The cloud cell size ($\approx$ 800 m) matched the spatial scale of upwelling radiances measured in the Coastal Stratus Experiment. Figure 18 is representative of the similar cloud structure at the end of the integration time for the in-cloud radiative forcing experiments. In Figure 19 a two-cell circulation pattern is seen because the buoyancy flux profile is altered by above-cloud cooling.

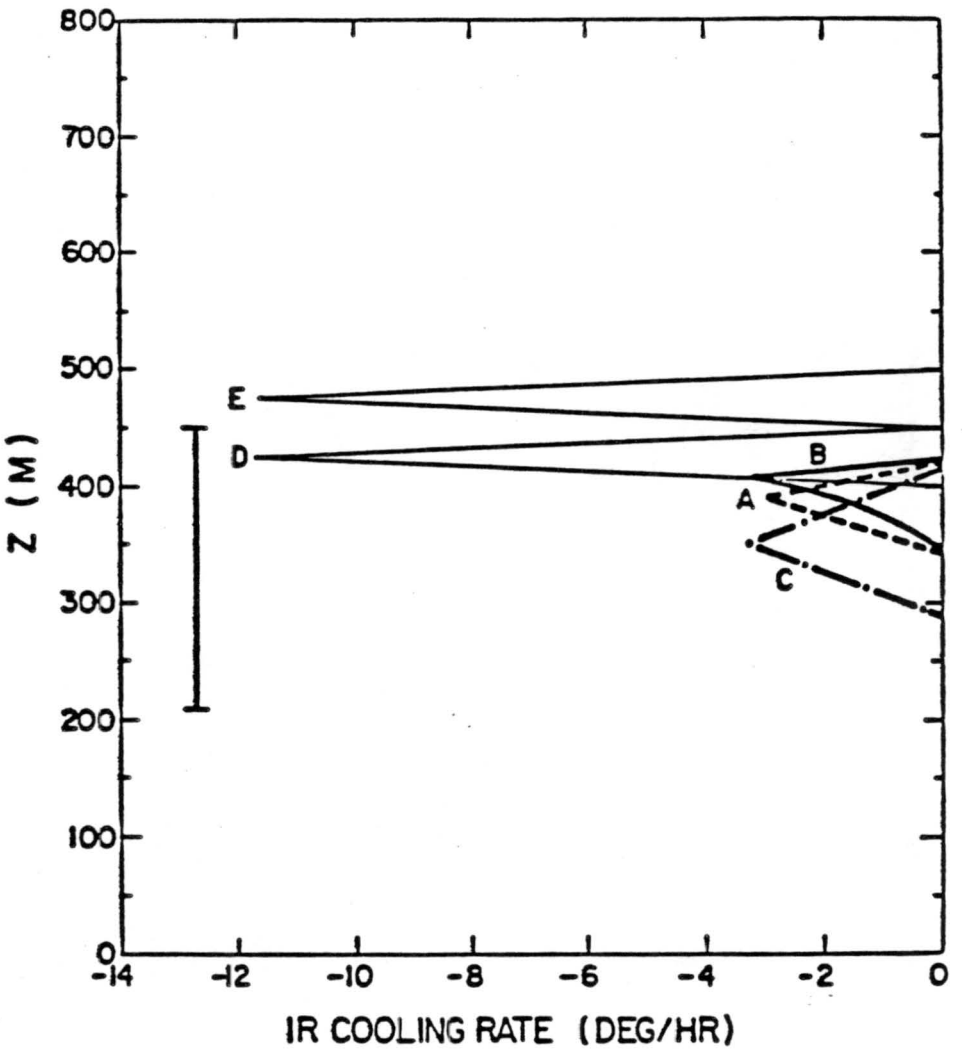

Figure 17: Five different profiles of infrared radiation cooling forcings used in the numerical experiments. The vertical bar indicates the vertical extent of cloud at the initial time (from Kuo, 1987).

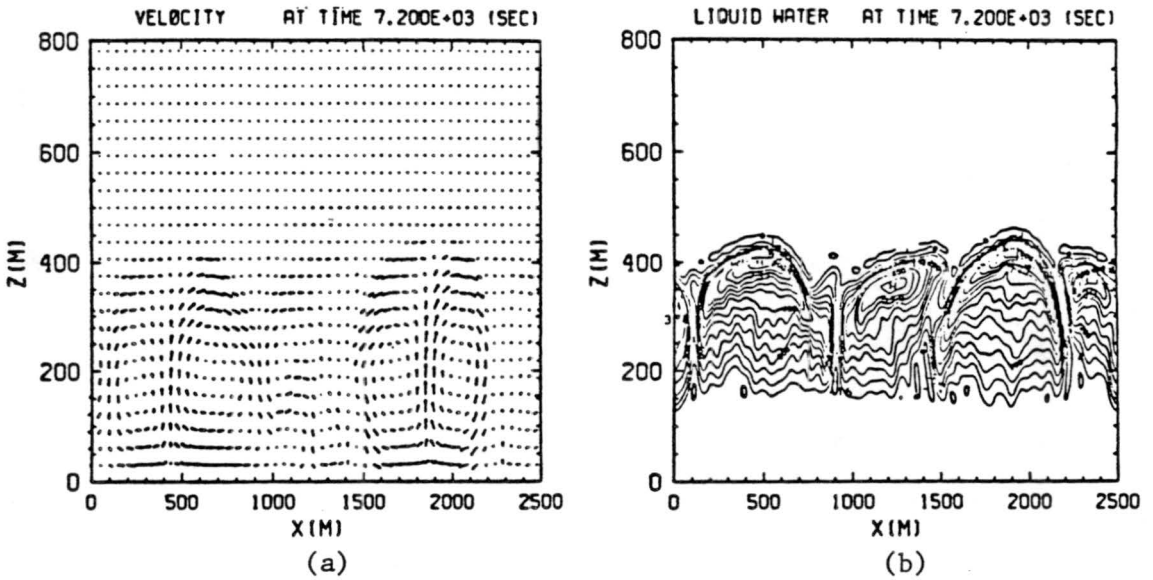

Figure 18: The velocity (a) and the liquid water mixing ratio (b) fields in the physical domain for an in-cloud radiation forcing. The liquid water mixing ratio lines are labeled in g kg^{-1} multiplied by 1000. Arrows in the velocity field are scaled to the maximum velocity (2.80 m s^{-1}).

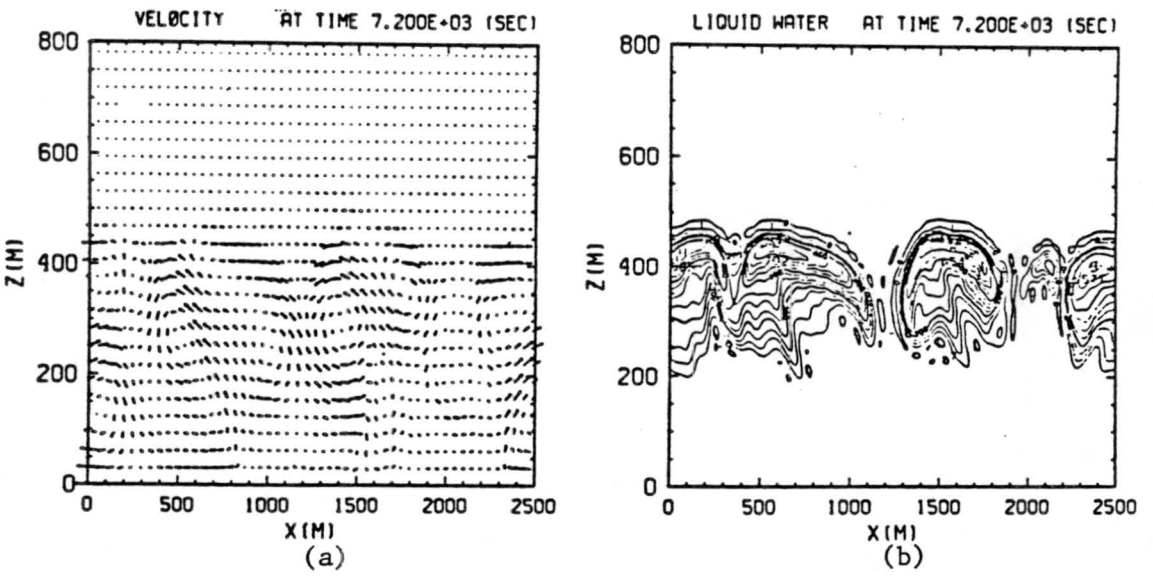

Figure 19: As in Figure 18, for the above-cloud radiation forcing. Maximum velocity for scaling in (a) is 1.57 m s^{-1}.

The sensitivity of the mixed layer dynamics to infrared cooling appears to be primarily related to the vertical positioning of this cooling relative to the cloud top. Flux profiles and cloud scale structure are insensitive to the horizontal or vertical variability in infrared cooling as long as it is confined to the turbulent cloud layer. Thus, the use of simple parameterizations for longwave flux seems to be justified. A continuation of this work should include a coupling of the dynamical model with radiative transfer schemes which can represent the longwave and shortwave components of the spatially inhomogeneous stratocumulus.

5.0 Summary of Preliminary Results

We can combine the results of the individual studies described in Sections 2, 3 and 4 to improve our knowledge of marine boundary layer variability. First, we have shown that the potential exists for discriminating cloud droplet size using cloud reflectance measurements in the 1.6 μm spectral window. Additional work needs to be done on the sensitivity of this method, and it's validation is necessary because this 1.6 μm channel will be transmitted from the upcoming AVHRR-K/L/M satellite series during daylight hours (rather than the 3.7 channel, which will be available only at night). Variations in droplet size have been indicated in some 3.7 μm imagery from AVHRR, in areas where island wakes were disturbing boundary layer mixing (Wetzel and Vonder Haar, 1985). The same patterns may be seen in the future near-infrared channel.

The presence of aerosol in the MABL also plays a role in boundary layer evolution and remote sensing. Although our radiative transfer modeling shows that the expected aerosol populations will not significantly influence cloud radiance selectively in the near-infrared, and hence not degrade the proposed remote sensing technique for cloud droplet size, the aerosol itself can help determine droplet size. As we have seen by the formation of cloud trails by ship effluent (Wetzel and Vonder Haar, 1986b), natural aerosol efficient at forming stratocumulus may often be lacking. The field measurements we obtained of aerosol size distributions showed low concentrations (40 cm^{-3}) of aerosol above the MABL, separated by the inversion from moderate to high concentrations (100–440 cm^{-3}) at cloud top. Maximum aerosol concentrations were found at cloud tops and near the ocean surface, suggesting aerosol primary sources to be evaporation from cloud droplets and ocean surface generation. It has been shown that aerosol optical depth can be estimated from satellite observations (Durkee *et al.*, 1984). Thus, we should attempt to relate cloud depths and droplet sizes, estimated from multi-channel radiance measurements, to aerosol optical depths existing prior to cloud formation and following cloud dissipation.

The distribution of moisture within the boundary layer is also dependant on cloud and aerosol (haze) processes. The dynamical modeling results described in Section 4.0 demonstrate that if

significant infrared cooling occurs in a (haze) layer above cloud, a two-cell circulation is established in the MABL, in contrast to the well-mixed layer for clouds with cooling confined to the cloud itself. Large concentrations of aerosol may induce this change. Remote sensing offers the opportunity to identify aerosol that can act as a moisture "sink" through hydration, and clouds that act as an aerosol "sink" through droplet activation and eventual precipitation.

The sensitivity of cloud dynamics to shortwave radiation transfer for differing cloud structure must also be known more precisely, in order to determine requirements for remote sensing. Although the dynamical model of Section 4.0 predicts that the horizontal and vertical distribution of cloud water has a small effect on infrared net flux, the horizontal distribution of cloud water determines shortwave optical depth and hence solar absorption in and below cloud. The satellite image sampling analysis of Section 3.0 concludes that full resolution GOES or AVHRR visible data (1 km resolution), or a routine data source with better spatial resolution, are needed to accurately determine cloud cover. Results of the Monte Carlo radiative transfer model (Section 2.3) show limited effect of cloud breaks for upward-directed radiances, but energy loss through side-scattering becomes significant for clouds of optical depths >10 and for calculations of net flux applied to thermodynamic energy budgets.

This research program has provided observations of the coastal stratus environment against which we can study remote sensing strategies for the MABL.

The work during the first 16 months of this 32-month research period show excellent results in both *in situ* and remote sensing observations, and in use of models to explore the observations. Appendix B is a list of papers supported under the grant. Thus we intend to propose continuing scientific studies of the MABL variability, with additional data from the FIRE Project and other sources.

Acknowledgements

We appreciated support of the NOAA ISCCP research project #NA-85-RAH-05-045 for some of the satellite data sets and computer processing. The Colorado State University Supercomputing Project provided funds for the use of the Cyber 205 supercomputer. Additional computer facilities were made available by CIRA and the National Park Service. The Naval Ocean Systems Center supported a large part of the field program, and we thank especially Dr. Doug Jensen. We continue to enjoy collaboration in this research with Dr. Phil Durkee at the U.S. Naval Postgradutate School. Dr. Chris Johnson of the National Park Service group in Fort Collins kindly provided efficient versions of some of the radiation codes.

REFERENCES

Battalino, T.E., R. Helvey, C.J. Walcek, J. Rosenthal, and J. Gottschalk, 1982: Air mass trajectory analysis as an aid in distiguishing marine from continental aerosol distributions at San Nicholas Island. In *Atmospheric Aerosols*, ed. A. Deepak. Spectrum Press, Hampton, VA, 125–134.

Caughey, S.J., and M. Kitchen, 1984: Simultaneous measurements of the turbulent and microphysical structure of nocturnal stratocumulus cloud. *Quart. J. Roy. Meteor. Soc.*, **110**, 13–34.

Collins, D.G., W.G. Blättner, M.B. Wells, and H.G. Horak, 1972: Backward Monte Carlo calculations of the polarization characteristics of the radiation emerging from spherical-shell atmospheres. *Appl. Opt.*, **11**, 2684–2696.

Davies, R., 1978: The effect of finite geometry on the three-dimensional transfer of solar irradiance in clouds. *J. Atmos. Sci.*, **35**, 1712–1725.

Davis, J.M., T.B. McKee, and S.K. Cox, 1985: Application of the Monte Carlo method to prblems in visibility using a local estimate: an investigation. *Appl. Opt.*, **24**, 3193–3205.

Durkee, P.A., E.E. Hindman, and T.H. Vonder Haar, 1984: The detection of marine haze with meteorological satellites. In Hygroscopic Aerosols in the Planetary Boundary Layer, ed. L.H. Ruhnke and A. Deepak, A. Deepak Publishing, Hampton, VA, 171–180.

Grant, I.P., and G.E. Hunt, 1968: Solution of radiative transfer problems in planetary atmospheres. *Icarus*, **9**, 526–534.

Hänel, G., 1976: The single-scattering albedo of atmospheric aerosol particles as a function of relative humidity. *J. Atmos. Sci.*, **33**, 1120–1124.

Jensen, D.R., 1978: Aerosol measurements in the marine boundary layer at San Diego. *Tech. Report 168*, Naval Ocean Systems Center, San Diego.

Kneizys, F.X., E.P. Shettle, W.O. Gallery, J.H. Chetwynd, Jr., L.W. Abreu, J.E.A. Selby, S.A. Clough, and R.W. Fenn, 1983: Atmospheric Transmittance/Radiance: Computer Code LOWTRAN 6. *AFGL Technical Report 83-0187*, 200 pp.

Kuo, H.-C., 1987: Dynamical modeling of marine boundary layer convection. *CSU Atmospheric Science Paper No. 412*, Colorado State University, 126 pp.

Nicholls, S., and J. Leighton, 1986: An observational study of the structure of stratiform cloud sheets: Part I. Structure. *Quart. J. Roy. Meteor. Soc.*, **112**, 431–460.

Nicholls, S., and J.D. Turton, 1986: An observational study of the structure of stratiform cloud sheets: Part II. Entrainment. *Quart. J. Roy. Meteor. Soc.*, **112**, 461–480.

Shettle, E.P., and R.W. Fenn, 1979: Models for the aerosols of the lower atmosphere and the effects of humidity variations on their optical properties. *Environmental Research Paper* **676**, AFGL-TR-79-0214, Air Force Geophysics Laboratory, Hanscom AFB, MA, 94 pp.

Shih, C.-F., and T.H. Vonder Haar, 1986: Comparison of diurnal characteristics of stratocumulus clouds over California and South America coasts using GOES satellite data. *Preprints, AMS Second Conf. on Satellite Meteorology/Remote Sensing*, Williamsburg, VA, 282–283.

Shih, C.-F., G.G. Campbell, and T.H. Vonder Haar, 1986: Effects of data resolution on satellite cloudiness estimation. *Preprints, AMS Second Conf. on Satellite Meteorology/Remote Sensing*, Williamsburg, VA, 398–401.

Shih, C.-F., M. Wetzel, and T.H. Vonder Haar, 1988: Effects of data resolution on marine stratiform cloud detection using AVHRR and VISSR satellite data. *Preprints, AMS Third Conf. on Satellite Meteorology and Oceanography*, Anaheim, CA, 401–403.

Slingo, A., and H.M. Schrecker, 1982: On the shortwave radiative properties of stratiform water clouds. *Quart. J. Roy. Meteor. Soc.*, **108**, 407–426.

Stephens, G.L., and C.M.R. Platt, 1987: Aircraft observations of the radiative and microphysical properties of stratocumulus and cumulus cloud fields. *J. Clim. Appl. Meteor.*, **26**, 1243–1269.

Twomey, S., and T. Cocks, 1982: Spectral reflectance in the near-infrared: Comparison of measurements and calculations. *J. Meteor. Soc. Japan*, **60**, 583–592.

Wetzel, M., and T.H. Vonder Haar, 1985: Use of existing and suggested satellite observations of reflected spectral radiance to estimate properties of stratiform clouds. In Report of the JSC/CAS Workshop on Modelling of Cloud Topped Boundary Layer. WMO/TD No. 75, WCP-106, Appendix G, 13–17.

Wetzel, M., and T.H. Vonder Haar, 1986a: The impact of stratocumulus microphysical variations on near-infrared radiance. *Extended Abstracts, AMS Sixth Conf. on Atmos. Radiation*, Williamsburg, VA, 153–156.

Wetzel, M., and T.H. Vonder Haar, 1986b: Modeling and observation of near-IR cloud signatures in the marine boundary layer. *Presentations at the Fourth Tri-Service Cloud Modeling Workshop*, Hanscom AFB, MA, 50–64.

Appendix A: Summary of Data from the Coastal Stratus Experiment

The Piper Navajo instrumented aircraft was directed on constant-altitude sampling passes within and above cloud during the field experiment. Spiral descents and ascents were also flown in order to obtain vertical thermodynamic profiles within the lower troposphere. Figures 20 through 25 are the temperature and dewpoint profiles obtained from the aircraft spirals. Cloud microphysical data for the clouds sampled during these flights are listed in Tables 3 through 5. The comparison of tabulated data to the vertical profiles can be made by matching the Julian date shown in the figure titles to those in the tables. The Figure 21 sampling period coincides most closely with case 177A in Table 3, Figure 22 coincides with case 178A and Figure 23 with case 180A. The profile in Figure 24 was made while descending to land at Montgomery Field, and few miles inland. Figure 25 corresponds to case 181A. Local sun (standard) time is eight hours behind the UTC times given in the figures.

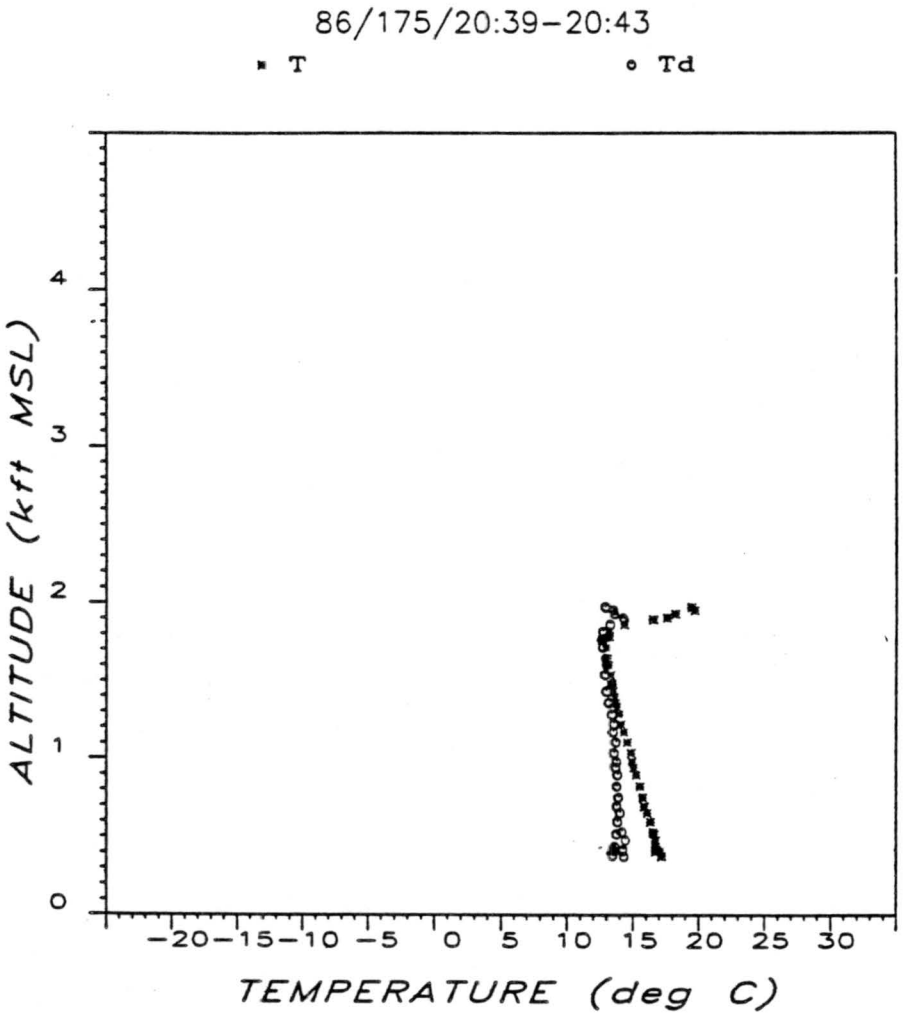

Figure 20: Temperature and dew point profile obtained by aircraft sampling on 1986 Julian day 175, during the UTC time period at the top of the figure.

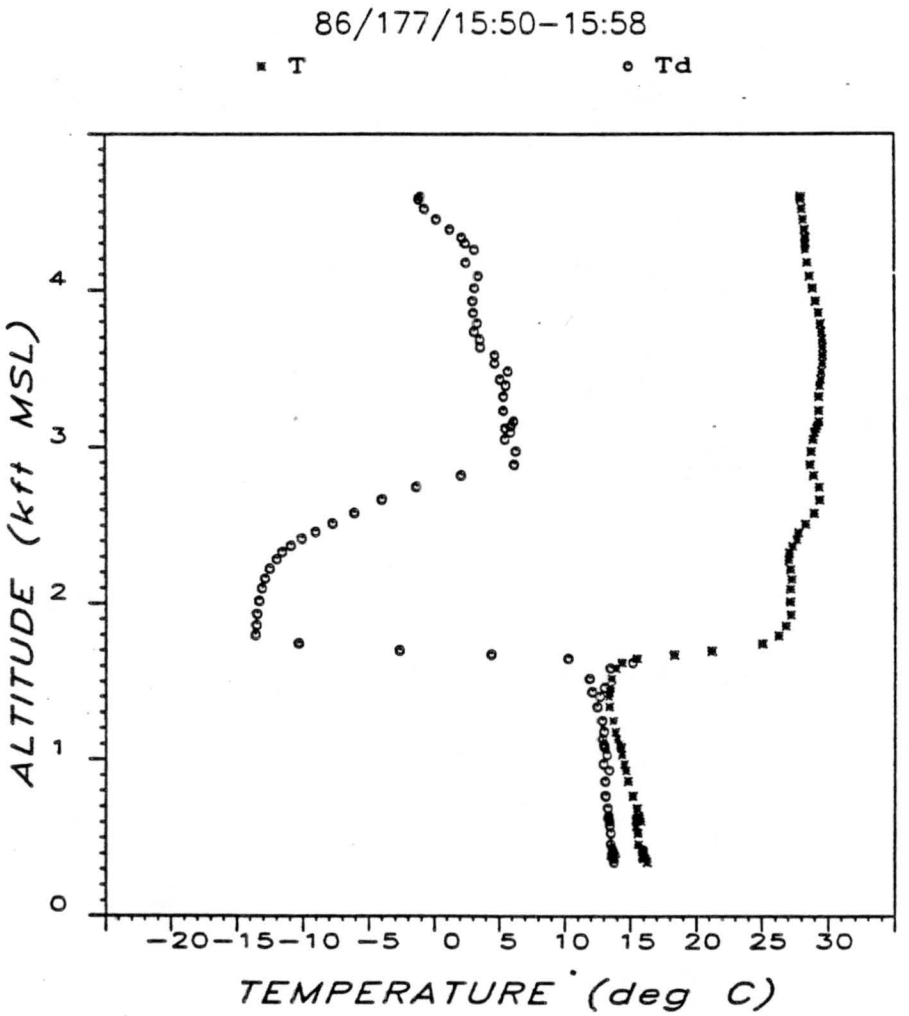

Figure 21: As in Figure 20, for day 177.

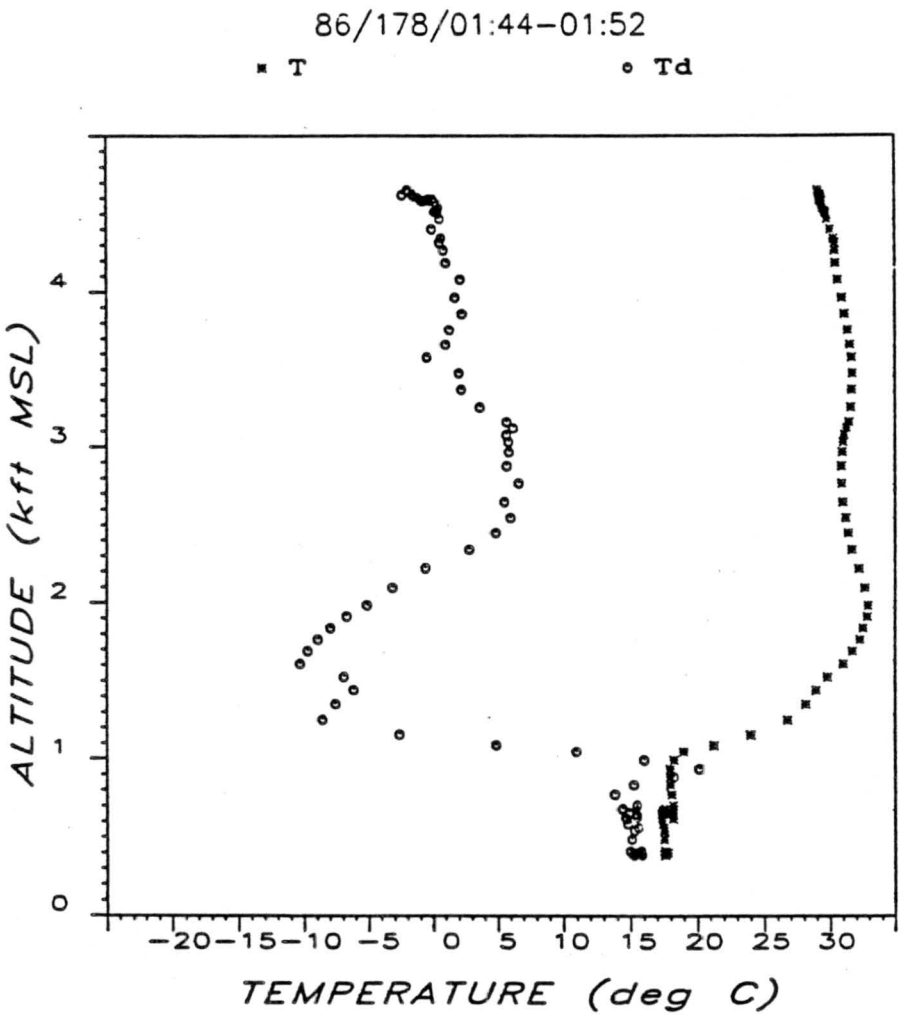

Figure 22: As in Figure 20, for day 178.

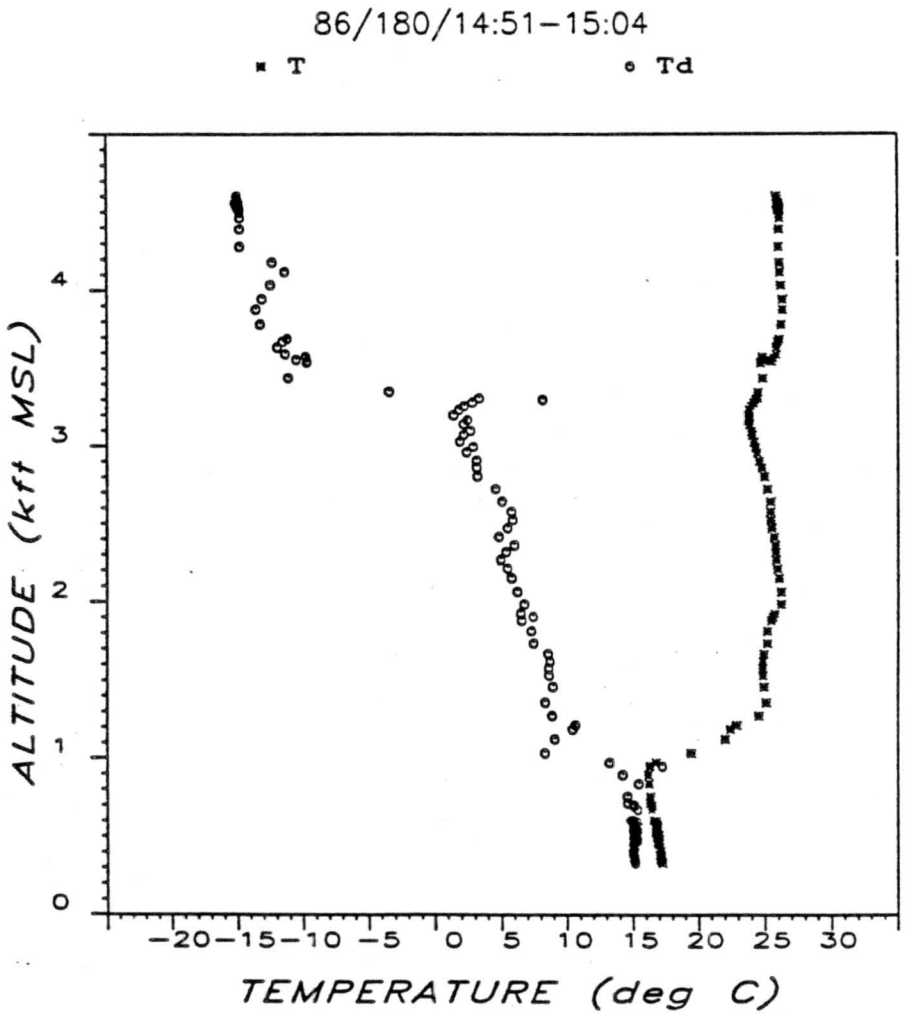

Figure 23: As in Figure 20, for day 180.

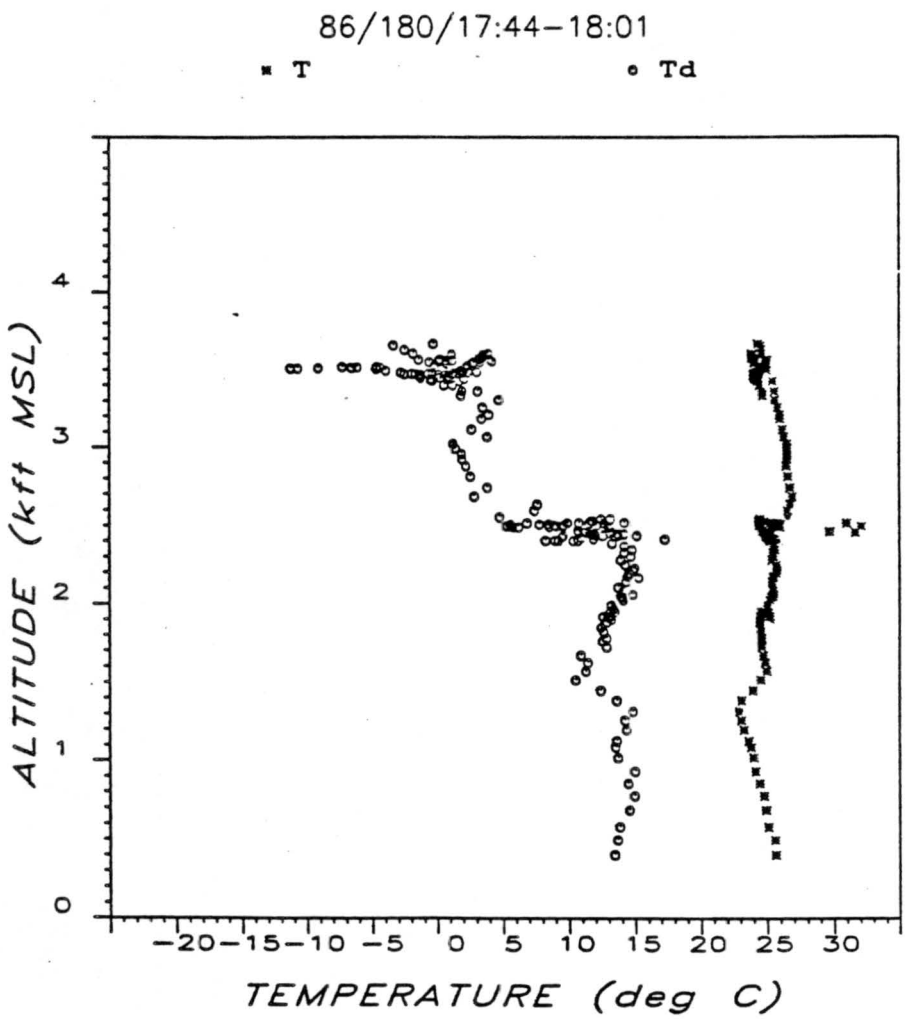

Figure 24: As in Figure 20, for day 180.

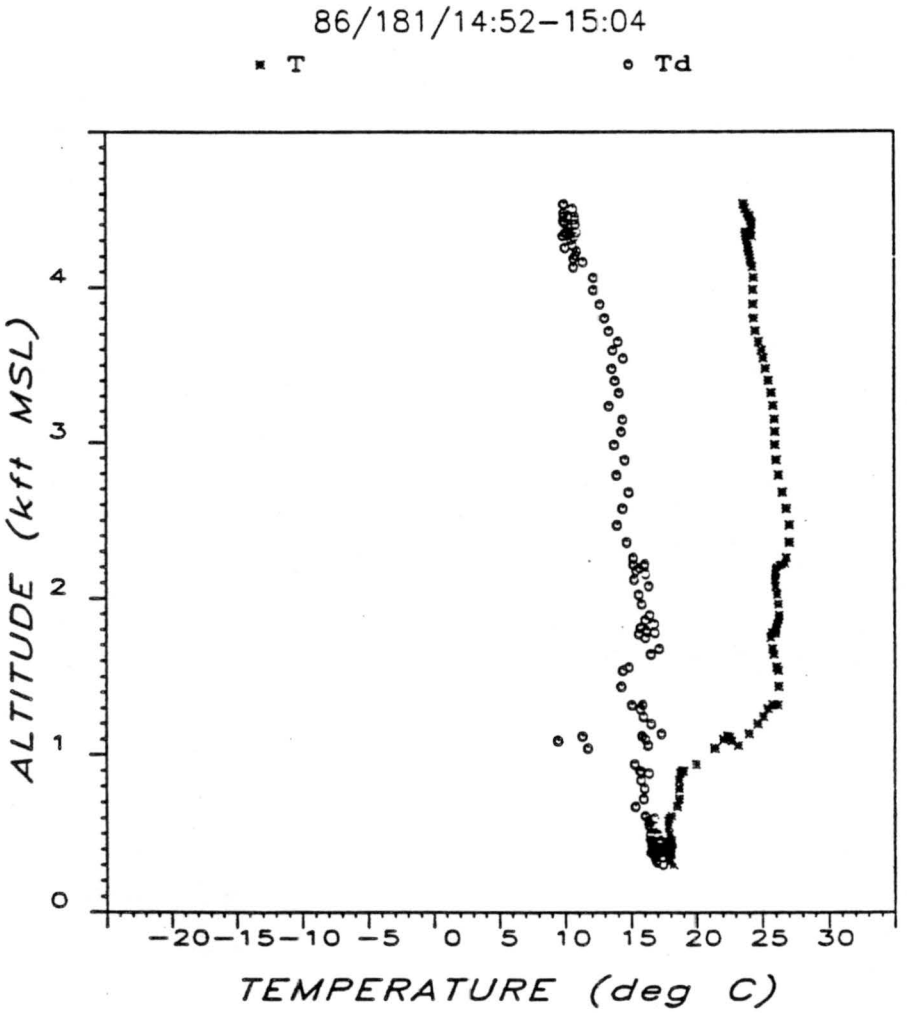

Figure 25: As in Figure 20, for day 181.

Table 3: Mean and dispersion values for size distributions on Julian days 175–178.

Label	*Z* (kft)	*Description*	$\overline{r_e}$ (μm)	D_{r_e}	$\overline{W}$ ($g\ m^{-3}$)	D_W	$\overline{N}$ (cm^{-3})	D_N
175A	1.7	Cloud top	4.69	0.532	0.114	0.822	377	0.373
	1.6	Below top	4.78	0.479	0.080	0.803	346	0.307
	1.4	In cloud	4.78	0.142	0.052	0.511	334	0.178
177A	1.8	Above cloud	0.314	0.083	<0.001	0.353	41	0.270
	1.5	Cloud tops	1.65	1.45	0.004	2.50	99	0.586
	1.4	Upper cloud	4.93	0.297	0.088	0.457	337	0.226
	1.3	In cloud	5.21	0.086	0.063	0.308	316	0.120
	1.2	In cloud	4.40	0.143	0.028	0.271	295	0.097
177B	1.4	Cloud top	5.41	0.091	0.113	0.333	339	0.169
	1.3	In cloud	5.37	0.079	0.096	0.231	321	0.088
	1.2	In cloud	4.50	0.158	0.033	0.349	309	0.115
	1.1	In cloud	3.62	0.183	0.014	0.654	302	0.099
178A	1.5	Above haze	0.316	0.105	<0.001	0.244	48	0.236
	1.0	At inversion	0.324	0.064	<0.001	0.735	135	0.584
	1.0	Occn'l Sc	0.310	0.014	<0.001	0.317	77	0.299
	1.0	Scattered Sc	0.857	1.47	<0.001	2.64	244	0.471
	0.8	Tenuous Sc	0.529	0.109	<0.001	0.247	439	0.156
	0.4	In haze	0.732	0.846	<0.001	1.16	256	0.197
	0.1	In haze	0.518	0.179	<0.001	0.262	523	0.228

Table 4: Mean and dispersion values for size distributions on Julian day 180.

Label	*Z* (kft)	*Description*	$\overline{r_e}$ (μm)	D_{r_e}	$\overline{W}$ ($g\ m^{-3}$)	D_W	$\overline{N}$ (cm^{-3})	D_N
180A	1.2	Cloud top	0.567	0.243	<0.001	0.502	436	0.180
	1.1	Upper cloud	5.68	0.400	0.075	0.764	249	0.247
	1.0	In cloud	6.38	0.066	0.110	0.224	245	0.125
	1.0	In cloud	6.34	0.057	0.103	0.197	257	0.114
	0.9	In cloud	5.91	0.083	0.089	0.271	269	0.080
	0.7	Lower cloud	11.58	0.216	0.554	1.15	341	0.117
	0.5	Cloud base	4.02	0.682	0.003	1.21	433	0.295
180B	1.8	Above haze, St	0.317	0.031	<0.001	0.193	93	0.209
	1.4	Above haze, St	0.315	0.033	<0.001	0.189	86	0.172
	1.2	Above haze, St	0.310	0.016	<0.001	0.192	78	0.186
	1.0	Above haze, St	0.321	0.095	<0.001	0.725	86	0.580
	0.9	Cloud tops	2.09	1.12	0.019	2.16	247	0.468
	0.8	Upper cloud	3.08	0.834	0.038	1.37	381	0.180
	0.7	In cloud	3.79	0.317	0.019	0.739	357	0.149
	0.6	Lower cloud	2.74	0.541	0.005	0.905	297	0.123
180C	1.4	Above St	0.338	0.275	<0.001	0.300	74	0.175
	1.2	Above St	0.316	0.067	<0.001	0.238	72	0.209
	1.0	Cloud tops	3.13	0.934	0.030	1.95	322	0.390
	0.9	Upper cloud	6.07	0.079	0.158	0.323	376	0.192
	0.8	In cloud	5.60	0.110	0.076	0.298	312	0.124
	0.7	Lower cloud	4.24	0.274	0.020	0.781	271	0.101

Table 5: Mean and dispersion values for size distributions on Julian day 181.

Label	Z (kft)	*Description*	$\overline{r_e}$ (μm)	D_{r_e}	$\overline{W}$ ($g\ m^{-3}$)	D_W	$\overline{N}$ (cm^{-3})	D_N
181A	1.1	Above haze	0.507	0.094	<0.001	0.302	439	0.258
	0.9	Above St	0.556	0.056	<0.001	0.185	407	0.165
	0.8	Near tops	5.19	0.442	0.045	0.987	227	0.172
	0.7	In cloud	6.63	0.089	0.103	0.327	311	0.100
	0.6	In cloud	6.17	1.17	0.097	0.396	374	0.098
	0.4	Lower cloud	5.45	0.196	0.107	0.435	940	0.094
181B	1.3	Above St	0.370	1.07	<0.001	0.543	139	0.433
	1.0	In some tops	1.93	1.35	0.006	2.57	265	0.373
	0.9	Cloud top	4.73	0.572	0.040	1.17	329	0.196
	0.8	In cloud	6.64	0.199	0.064	0.553	256	0.096
	0.7	In cloud	6.21	0.221	0.074	0.566	264	0.102
	0.6	Lower cloud	5.55	0.369	0.060	0.628	440	0.755
181C	1.2	Haze top	0.374	0.058	<0.001	0.497	197	0.393
	1.1	Above St	0.403	0.079	<0.001	0.531	256	0.386
	1.0	Above St	0.953	2.22	0.014	3.73	235	0.317
	0.9	Through turret	1.21	1.43	0.008	2.57	375	0.071
	0.8	Through turret	1.16	0.845	<0.001	1.33	322	0.119

Appendix B: Cumulative List of Reports, Publications and Presentations

Included below are those reports, publications and presentations which have been prepared in conjunction with this program of research.

Kuo, H.-C., and T.H. Vonder Haar, 1986: Radiation effects on a Boussinesq boundary layer model. *Preprints, 6th Conf. Atmos. Radiation*, Amer. Meteor. Soc., Boston, 35–38.

Kuo, H.-C., 1987: Dynamical modeling of marine boundary layer convection. *CSU Atmospheric Science Paper No. 412*, Colorado State University, 126 pp.

Shih, C.-F., and T.H. Vonder Haar, 1986: Comparison of diurnal characteristics of stratocumulus clouds over California and South America coasts using GOES satellite data. Second Conference on Satellite Meteorology/Remote Sensing and Applications, American Meteorological Society. May 13-16, 1986. Williamsburg, VA.

Shih, C.-F., G.G. Campbell, and T.H. Vonder Haar, 1986: Effects of data resolution on satellite cloudiness estimation. Second Conference on Satellite Meteorology/Remote Sensing and Applications American Meteorological Society. May 13-16, 1986. Williamsburg, VA.

Shih, C.-F., M. Wetzel, and T.H. Vonder Haar, 1988: Effects of data resolution on marine stratiform cloud detection using AVHRR and VISSR satellite data. Third Conference on Satellite Meteorology and Oceanography. American Meteorological Society. January 31- February 5, 1988. Anaheim, California.

Vonder Haar, T.H., 1986: Semi-Annual Report to ONR on Contract #N00014–86–C–0459. Cooperative Institute for Research in the Atmosphere, 22 pp.

Wetzel, M., and T.H. Vonder Haar, 1986a: The impact of stratocumulus microphysical variations on near-infrared radiance. *Extended Abstracts, AMS Sixth Conf. on Atmos. Radiation*, Williamsburg, VA, 153–156.

Wetzel, M., and T.H. Vonder Haar, 1986b: Modeling and observation of near-IR cloud signatures in the marine boundary layer. *Presentations at the Fourth Tri-Service Cloud Modeling Workshop*, Hanscom AFB, MA, 50–64.

Appendix C: Graduate Student Support

Those graduate students supported in part or in full by this project are listed below. Degrees recently granted to students participating in the research are also shown.

1. Students Supported

   Hung-chi Kuo, CSU Department of Atmospheric Science

   Chi-Fan Shih, CSU Department of Atmospheric Science

   Melanie Wetzel, CSU Department of Atmospheric Science

2. Degrees Granted

   Hung-chi Kuo, Ph.D. in Atmospheric Science (1987); his present affiliation is UCAR Postdoctoral Scientists, Naval Environmental Prediction Research Facility, Monterey, California.